Heliyon 9 (2023) e21524

Contents lists available at ScienceDirect

Heliyon

journal homepage: www.cell.com/heliyon

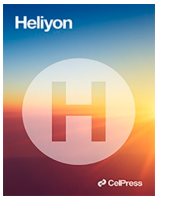

Effect of miR-182-5p on apoptosis in myocardial infarction

Nan Niu [b], Huangtai Miao [c], Hongmei Ren [a,*]

[a] Department of Cardiovascular Medicine, People's Hospital of Ningxia Hui Autonomous Region, Yinchuan, Ningxia Hui Autonomous Region, 750021, PR China
[b] College of Physics and Optoelectronic Engineering, Canghai Campus of Shenzhen University, Shenzhen, Guangdong, 518060, PR China
[c] Coronary Heart Disease Center, Beijing Anzhen Hospital, Capital Medical University, Beijing, 100029, PR China

ARTICLE INFO

Keywords:
Myocardial infarction
miR-182-5p
Myocardial hypoxia
Apoptosis

ABSTRACT

Objective: This study aimed to delineate the diagnostic significance of miR-182-5p by investigating its influence on myocardial apoptosis and function, employing both in vivo and in vitro myocardial infarction models.
Methods: A rat myocardial infarction model was established. Myocardial infarction area was detected using the 2,3,5-chlorotriphenyltetrazolium (TTC) method, myocardial enzyme spectrums were measured using enzyme-linked immunosorbent assay (ELISA), myocardial structure was detected by hematoxylin and eosin (HE) staining, myocardial apoptosis was detected using the TUNEL method, and expression levels of miR-182-5p and apoptosis-related molecules were detected using real-time fluorescence quantitative PCR (qPCR) and Western blot. miR-182-5p mimics and inhibitor were transfected into rat H9C2 cardiomyocytes and mouse HL-1 cardiomyocytes to establish a hypoxia model. Cardiomyocyte viability was detected using the CCK-8 method, expression levels of apoptosis-related indicators were detected using Western blot, and caspase-3/7 activity was detected using a caspase-3/7 activity detection kit. AAV9 adeno-associated virus was used to construct an miR-182-5p overexpression virus, which was injected into mice through the tail vein to create a mouse myocardial infarction model. TTC, ELISA, HE staining, echocardiography, real-time fluorescence qPCR, and Western blot methods were used to detect the effects of AAV9-miR-182-5p on myocardial injury, myocardial function, and myocardial apoptosis levels in myocardial infarction.
Results: The rat model displayed reduced miR-182-5p expression concurrent with an increase in apoptosis. The in vitro H9C2 and HL-1 hypoxia models revealed that miR-182-5p augmented the hypoxia-induced decrease in myocardial cell viability, suppressed Bcl-2 expression, and increased Bax, Bnip3, and caspase-3/7 activity levels. The injection of AAV9-miR-182-5p significantly exacerbated myocardial tissue damage, impaired myocardial function, and enhanced apoptosis.
Conclusion: miR-182-5p escalates myocardial injury during myocardial infarction by fostering apoptosis. Interventions that aim to reduce miR-182-5p levels might be crucial in halting the progression of myocardial infarction.

1. Introduction

Myocardial infarction (MI) stands out among cardiovascular diseases because of its grave implications and increasing prevalence

* Corresponding author.
E-mail address: nn2023fly@szu.edu.cn (H. Ren).

https://doi.org/10.1016/j.heliyon.2023.e21524
Received 14 July 2023; Received in revised form 21 October 2023; Accepted 23 October 2023
Available online 31 October 2023

[1]. The urgency of identifying effective MI treatments is driven by the pressing need to improve clinical outcomes, patient prognosis, and overall quality of life. As such, cardiovascular research, spanning both fundamental and clinical aspects, is gaining global momentum. Within this realm of research, the molecule miR-182-5p has come to the forefront.

MiR-182-5p is an endogenous short-chain non-coding RNA that functions transcriptionally, either by inhibiting translation or prompting the degradation of target mRNA. Its significant role in various cardiovascular pathologies, such as atherosclerosis, MI, and ventricular remodeling, has been underscored in recent studies [2]. Some researchers are even advancing the idea of miR-182-5p as a potential prognostic marker for chronic heart failure, introducing a new approach to the diagnosis, treatment, and prognosis of heart diseases [3,4]. However, its specific role in MI remains a subject of debate. Although certain studies suggest the protective role of miR-182-5p outside of MI, such as reducing vascular regeneration-induced myocardial hypertrophy and shielding against cardiac structural damage in diabetic cardiomyopathy [5,6], other in vitro experiments with rat H9C2 cardiomyocytes show its inhibition drastically reduces hypoxia-induced myocardial damage [7]. Animal studies further corroborate that inhibiting miR-182-5p lessens MI damage [8]. Yet, there are opposing views, with some research implying that increasing miR-182-5p expression may significantly reduce MI and promote myocardial survival [9]. Clearly, there's a need for clarity on miR-182-5p's function in ischemic and hypoxia-induced myocardial injury.

Delving into the intricacies of miR-182-5p's effects, especially in the context of MI, is critical. Apoptosis, chiefly characterized by ischemic and hypoxic myocardial cell death, plays a significant role in sustained myocardial cell loss post-MI, leading to severe complications like ventricular remodeling, heart failure, and sudden cardiac death [10,11]. To enhance MI treatment outcomes, research efforts are centered around curtailing myocardial apoptosis, making it a pivotal metric to gauge molecular and therapeutic responses. This sets the stage to understand miR-182-5p's influence on MI-induced apoptosis. Our study sought to decode this relationship, utilizing both in vitro and in vivo MI models. We exposed rat H9C2 and mouse HL-1 cardiomyocytes to hypoxic conditions to discern the effects of miR-182-5p on myocardial proliferation and apoptosis. Additionally, to evaluate its role post-MI, mice were given an AAV9-miR-182-5p overexpression injection. The outcomes of these exhaustive experiments endorse miR-182-5p as a valuable diagnostic and therapeutic target for MI, paving the path for subsequent detailed explorations into its molecular implications in MI.

2. Materials and methods

2.1. Cell culture

H9C2 embryonic rat heart-derived cells and HL-1 mouse cardiomyocytes were purchased from the Shanghai Chinese Academy of Sciences cell bank. Cells were cultured in Dulbecco's modified Eagle's medium (DMEM) with 10% fetal bovine serum under 5% carbon dioxide and normoxic conditions. When cells reached 80% confluence, 0.25% trypsin containing EDTA was used for digestion, and the cells were passaged. The experiment was conducted at approximately 60%–80% cell confluency.

2.2. Experimental animals

Thirty-six SPF grade adult healthy male Sprague–Dawley (SD) rats aged 6–8 weeks, weighing 200–250 g, were provided by Chengdu Dashuo Experimental Animal Co., Ltd. SD rats were allowed free access to food and water at a temperature of 23–25 °C after being acclimated, and were fed adaptively for one week before entering the experiment. The rats were divided into two groups: the sham-operated group (Sham) and the ischemic cardiomyopathy group (Model).

Approximately eight-week old, male, SPF grade C57BL/6 mice (n = 60), weighing around 20 g were purchased from Sibeifu (Beijing) Biotechnology Co., Ltd. All animals were raised in cages at the Beijing Maide Connor Animal Experimental Center, with an ambient temperature of 20–25 °C, a relative humidity of 60%, and 12 h alternating light and dark cycle. The drinking water and cages were sterilized using high-pressure sterilizers. The feed and bedding were irradiated. The feed and water were freely available, and the bedding was replaced once a day. Animals were adaptively fed in animal rooms for seven days before experimental modeling.

2.3. Myocardial infarction model

2.3.1. Rat myocardial infarction model

Male SD rats, weighing 150–200 g were selected. The rats were anesthetized using ether inhalation, and their skin was incised. Hemostatic forceps were used to open the chest cavity between the fourth and fifth ribs on the left edge of the sternum. Both sides of the chest cavity were gently compressed to allow the heart to protrude out of the chest cavity. The anterior descending branch of the left coronary artery was identified between the outflow tract of the pulmonary artery and the left atrium. A 0/6 non-invasive suture needle was used to thread a silk thread around the coronary artery of the left anterior descending branch (LAD), and then each end of the thread was passed through a small ethylene tube to form a trap, forming a living knot. The trap was pulled and the catheter was fixed with a mosquito clip. Temporary occlusion of LAD arteries led to local ischemia; subsequently, the heart was quickly repositioned through ligation with a 0/6 non-invasive suture needle and artificial chest compressions were performed for resuscitation. Death within 24 h after surgery was not included in the scope of this experiment. The suture in the sham-operated group only passed through the coronary artery without ligation, whereas the other steps remained the same. After 4 weeks of conventional feeding, the rats were used for experiments.

2.3.2. Mouse myocardial infarction model

The mice were anesthetized, and a small round needle with 6-0 non-absorbable silk thread was used to ligate the LAD of the left coronary artery at a distance of 2–3 mm from the lower edge of the left atrial appendage. After successful ligation, the apex of the heart instantly turned white, and hemostatic forceps were immediately used to open the incision and push the heart back into the chest cavity by tightening the pouch and closing the chest. The sham-operated group of mice underwent the same procedure without ligation of the left coronary artery.

2.3.3. Establishment of a myocardial hypoxia model

On the day before the hypoxia experiment, 2×10^6 cells were sub-cultured in a 60 mm cell culture dish and adhered overnight in a 37 °C incubator. On the second day, the oxygen concentration was first reduced to less than 1% using an oxygen-deficient operating platform. The complete culture medium was pretreated with nitrogen gas in the oxygen-deficient operating platform to remove oxygen. Then, the cells were placed on the oxygen-deficient operating platform for fluid exchange. After changing the liquid, the cells were placed in a three-gas incubator with a 1% oxygen concentration generated using an oxygen-deficient transfer chamber and cultured at 37 °C. After the completion of hypoxia, the cells were transferred to the hypoxia operating platform for experimentation.

2.3.4. Injection of adeno-associated virus

pAAV2 CMV_ BGI-EGFP-3xFlag was used to construct the miR-182-5p adeno-associated virus (AAV9-miR-182-5p); the process of virus construction was conducted by Sheweisi Biology (Tianjin, China). Viruses were collected and stored in a −80 °C refrigerator for later use. The mice were placed in the fixation tank, which contained several holes on the back through which the tail could pass. After the tail was passed through the holes, the tail vein was exposed. The tail vein was wiped with 75% alcohol to fully expand the tail vein. Purified adeno-associated virus (50 μL) with 2×10^{11} PFU was injected using a no. 4 needle. After 2 weeks of adaptive feeding, the vital signs of the mice were observed such as activity, eating, and drinking water. Mice with good growth status were sacrificed, and the expression levels of green fluorescence and miR-182-5p were observed in the myocardial tissue. Successfully identified mice were used for subsequent myocardial infarction analyses.

2.3.5. 2,3,5-Chlorotriphenyltetrazolium staining

After the animal was euthanized, the heart was immediately removed and the blood was flushed out with phosphate buffered saline (PBS). The extracted heart was placed in a −20 °C refrigerator for quick freezing for 15 min for easy slicing. The heart was sliced into five to six sections of 2 mm each. The slices were placed in 1% 2,3,5-chlorotriphenyltetrazolium (TTC) and incubated in a constant temperature water bath at 37 °C for approximately 30 min. The stained sections were then fixed in 4% paraformaldehyde for 24 h. The final product was photographed to detect the size of the infarct volume.

2.3.6. Hematoxylin-eosin staining

Tissue sections were stained with hematoxylin dye was performed for 10 min. The excess staining solution was rinsed with tap water for 5 min, then washed again with distilled water for a few seconds. Subsequently, staining with eosin dye was performed for 30 s. The excess dye solution was rinsed with tap water for 3 min, then washed again with distilled water. It was then sealed with neutral resin. Under the microscope, the nucleus was seen as blue, while the cytoplasm was red or pink.

2.3.7. TUNEL staining

After sampling, the tissue was cleaned with PBS and fixed with 4% paraformaldehyde, then soaked in ethanol and dehydrated for 10 min. The dehydrated tissues were then soaked in xylene for transparency for 10 min. Subsequently, the transparent treated tissue was soaked in melted paraffin for 3 h, which embedded it, and a microtome was used to cut the tissue in the paraffin block into thin slices with a thickness of 5 μm, and lay them flat on an anti-detachment glass slide. The slices were baked on a 55 °C heated surface, so that the tissue slides were tightly attached to the anti-detachment glass slide. Then, paraffin section dewaxing and rehydration were performed, 50 μl of TUNEL reaction mixture was added to the sample, and the slides placed in a humid box and incubated in a constant temperature incubator (37 °C) for 60 min. The sample was washed with PBS three times, each time for 3 min, then hematoxylin staining solution was used for nuclear staining. Finally, the sample was washed with PBS three times, sealed with neutral resin, and inspected under light microscopy.

2.3.8. Detection of myocardial enzyme spectrum

The experimental mice were weighed and anesthetized with 7% chloral hydrate intraperitoneal injection (5 mL/kg). The abdominal cavity was opened and the abdominal aorta was bled until death. The chest cavity was opened and the blood was washed from the heart tissue using ice cold PBS. The blood was then stored at −80 °C for myocardial zymogram detection. Rat creatine kinase (CK), and lactate dehydrogenase (LDH) were measured using commercial ELISA kits provided by Enzyme-linked Biotechnology Co., Ltd. (Shanghai, China). *Asparagus cochinchinensis* aminotransferase/glutamic oxaloacetic transaminase (AST/GOT) were measured using commercial ELISA kits provided by Nanjing Jiancheng Bioengineering (Nanjing, China). Troponin T (cTnT) was detected by ELISA kit provided by Jianglai Biology (Shanghai, China). Mouse muscle creatine kinase (CK), creatine kinase-myocardial band (CK-MB), and LDH were detected by ELISA kit provided by Wuhan Gene Beauty Technology Co., Ltd. (Wuhan, China). All indicators were evaluated according to the kit instructions.

2.3.9. Real-time fluorescence quantitative polymerase chain reaction

Total RNA samples were extracted using RNAiso reagents (Takara Bio,China) according to the instructions, after measuring the mass and concentration of RNA using an ultra-micro spectrophotometer. The expression of relative genes was detected using two-step real-time quantitative reverse-transcription polymerase chain reaction (qRT-PCR). Quantitative PCR was performed with SYBR Green Master Mix (TaKaRa, Otsi, Shiga, Japan) on a LightCycler480 II Real-Time PCR System (Roche, Roswell, GA, USA), and the data were quantified using the $2^{-\Delta\Delta\ Cq}$ method [12]. U6 was used as an internal reference control. The reaction conditions were pre-denaturation at 95 °C for 5 min, followed by 40 cycles of denaturation at 95 °C for 10 s, annealing at 60 °C for 30 s, and extension at 72 °C for 30 s. The primer sequences for miR-182 in H9C2 cells and mice were 5′-GGCGCUUUGGCAAUGGUAGAACU-3′ (forward), and 5′-CCTCTAGGACCTGGATACTCTC-3′ (reverse). The primer sequences for miR-182 in HL-1 cells and mice were 5′-UUUGGCAAUGGUAGAACU-3′ (forward), and 5′-CTCAACTGGTGTCGTGGA-3′ (reverse).

2.3.10. Western blot

For Western blot (WB) analysis, RIPA lysate containing protease inhibitor was prepared. The composition of the lysate was: 50 mM Tris HCL, 150 mM NaCl, 1% Triton X, 1% sodium deoxycholate, 0.1% SDS, and 5 mM EDTA. The components of protease inhibitor were 2 μg/mL aprotinin, 1 mmol/L PMSF, and 1 μg/mL leupeptin. These reagents were all purchased from Sigma Aldrich Co. (St. Louis, MO, USA). All experimental operations were conducted on ice. After protein lysis, the BCA method was used for quantification; a total protein sample of 30 ng was used. The electrophoresis conditions were 120 V for 15 min, 150 V for 55 min, and the membrane transfer conditions were subjected to a constant current of 300 mA for 2 h. The membrane was blocked with PBS-T containing 5% skim milk powder for 1 h, and incubated with the primary antibody overnight. Antibodies against the following proteins and dilutions were as follows: HIF-1 α (NB100-105, 1:1000; Novus Biologicals, Briarwood, CO, USA), β-actin (ab49900, 1:10,000, HRP condensed; Abcam, Cambridge, UK), Bcl-2 (26,593 1-ap, 1:1000; Proteintech, Rosemont, IL, USA), Bax (ab32503, 1:2000; Abcam), Bnip3 (ab109362, 1:1000; Abcam), P53 (ab26, 1:1000; Abcam), caspase-3 (19677 1-AP, 1:500; Proteintech), cleared caspase-7 (# 8438, 1:500; Cell Signaling Technology (CST), Danvers, MA, USA), and cleared PARP (# 9542, 1:500; CST). On the second day, after washing the membrane, goat anti-rabbit (1:25,000, Bios Antibodies, Beijing, China) and goat anti-mouse (1:25,000, Bios Antibodies) antibodies were applied and incubated for 4 h. A ChemiDoc MP Imaging System (Bio-Rad Laboratories, Hercules, CA, USA) was used for protein imaging.

2.3.11. Transfection of miR-182 mimics and inhibitor

miR-182-5p mimic, miR-182-5p inhibitors, and control were purchased from Zixi Biotech Co., Ltd. (Beijing, China). The RNA was transfected into H9C2 and HL-1 cells using Lipofectamine 3000 (Invitrogen, Carlsbad, CA, USA) following the manufacturer's protocols. After transfection, cells were kept overnight in a complete medium, then placed in a serum-free medium and used for the experiment.

2.3.12. Echocardiography

Echocardiography was performed using the Vevo 3100 high-resolution ultrasound imaging system produced by VisualSonics (Toronto, ON, Canada). Echocardiography was performed using an MX550 probe with a frequency of 30 MHz. The tested mice were anesthetized with isoflurane inhalation, and long-axis B-ultrasound and M-ultrasound images of the heart were obtained near the left sternum. The probe was rotated 90° to obtain short-axis B-ultrasound and M-ultrasound images at the papillary muscle level. The left ventricular anterior wall thickness (LVAWd, LVAWs), left ventricular posterior wall thickness (LVPWd, LVPWs), and left ventricular inner diameter (LVIDd, LVIDs) were measured at the end of diastole and end of systole, respectively, using left ventricular short axis ultrasound. The left ventricular volume (LVEDV, LVESV), ejection fraction (EF), and short axis shortening rate (FS) were calculated at the end of diastole and end of systole. All ultrasound measurements were taken as the average of three consecutive cardiac cycles.

2.3.13. Detection of cell apoptosis by flow cytometry

Fresh myocardial tissue was minced using ophthalmic scissors, and blood cells were removed by repeated washing with PBS. Trypsin and type II collagenase were applied for digestion in a 1:1 ratio. After complete digestion, a 300-mesh sieve was used for filtration, and fetal bovine serum was added to terminate digestion. The sample was centrifuged at 160 g/min for 10 min, then the supernatant was discarded. Subsequently, the sample was repeatedly blown and the cells were cleaned with phosphate buffer, to make a single-cell suspension of myocardial cells. A 100 μL cell suspension with a concentration of 5×10^6 cells/mL was combined with 5 μL annexinV-PE, 1 μL 7AAD solution, incubated on ice in the dark for 10 min, then 400 μL binding buffer was added and myocardial cell apoptosis detected within 30 min.

2.3.14. CCK-8 assay

Before testing, the cells were counted and the cell concentration was adjusted to 2×10^4 cells/mL, and the cells inoculated into a 96 well plate, with five multiple wells per group. The cells were then cultured overnight in a 37 °C cell incubator. On the second day, the cells were placed in a three-gas incubator with 1% O_2, 5% CO_2, and 94% N_2; cells cultured under normal conditions were set as the control group. A 10 μL CCK-8 working solution was added to each well after cultivation. Cultivation was continued in the incubator for 3 h, then the optical density (OD) value was measured at 450 nm using a microplate reader. After removing the maximum and minimum values, the average value of each group of results was taken, and the cell survival rate was calculated according to the following formula: Cell survival rate (%) = (hypoxia group OD value − blank group OD group)/(normal group OD value - blank pore OD value) × 100.

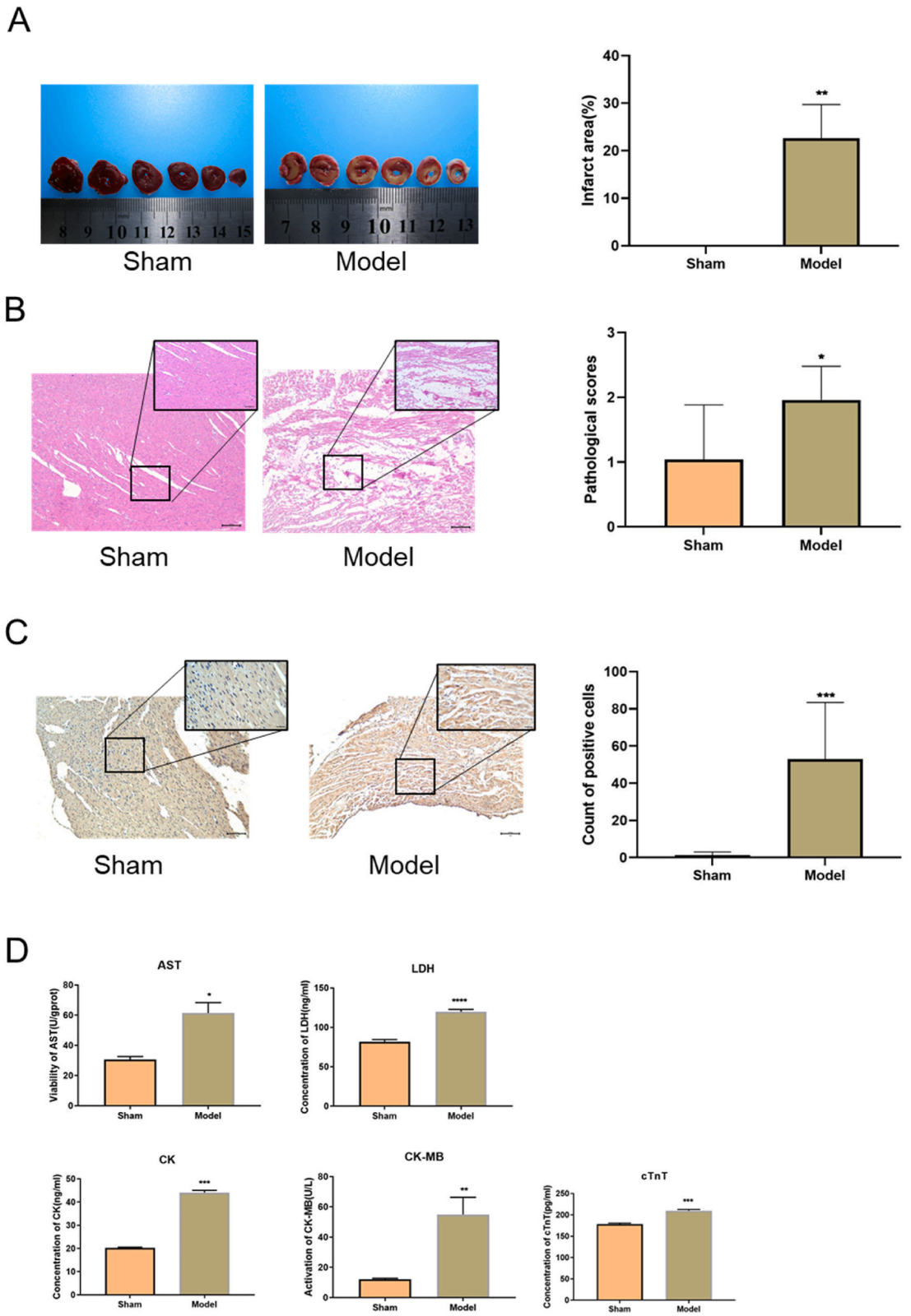

Fig. 1. Establishment of the rat myocardial infarction model. (A) The TTC method identified the myocardial infarction area. (B) Myocardial structure was visualized using HE staining (100×). (C) Cell apoptosis was determined by TUNEL (100×). (D) Myocardial enzyme-related molecules such as CK, CK-MB, LDH, cTnT, and AST were quantified using ELISA. (E) qPCR measured the expression level of miR-182-5p in myocardial tissue.

(F) Apoptosis-related molecules in myocardial tissue were determined by Western blot analysis. All data are represented as mean ± standard deviation (n = 6). Significant differences against the sham group are denoted by *$P < 0.05$, **$P < 0.01$, ***$P < 0.001$, ****$P < 0.0001$ versus the sham group. Legends: AST – aspartate aminotransferase; CK – creatine kinase; CK-MB – creatine kinase-MB; cTnT – cardiac troponin T; ELISA – enzyme-linked immunosorbent assay; LDH – lactate dehydrogenase; qPCR – quantitative polymerase chain reaction; TTC – 2,3,5-chlorotriphenyltetrazolium.

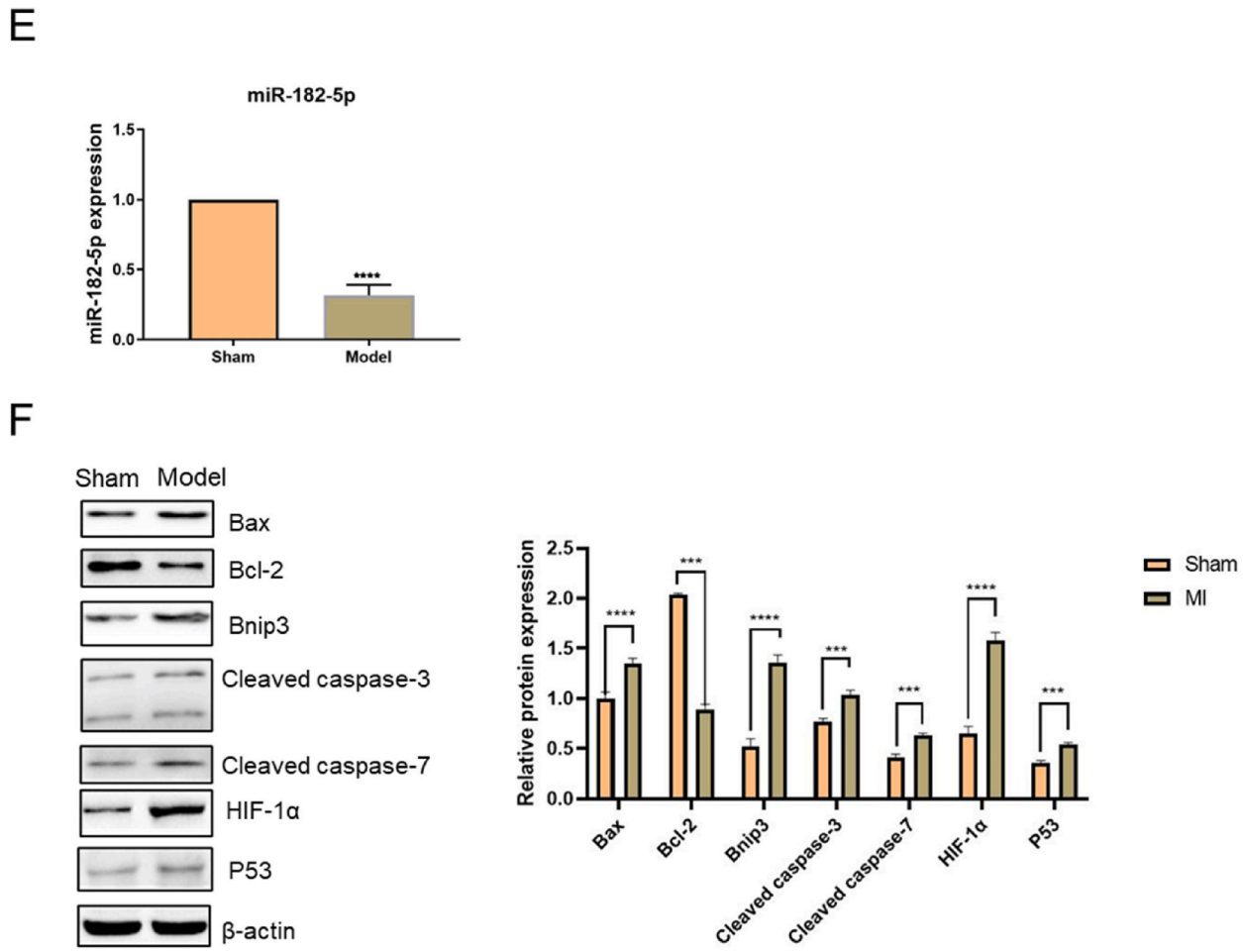

Fig. 1. (*continued*).

2.3.15. Statistical analysis

SPSS 17.0 (IBM Corporation, Armonk, NY, USA) was used for statistical analysis. The results are expressed as mean ± standard deviation. The Student's t-test was used to compare the mean between two samples, one-way ANOVA test was used to compare the mean between multiple samples, and the Student Newman–Keuls test was used to compare the mean between two groups. Statistical significance was set at $P < 0.05$.

3. Results

3.1. Establishment of the myocardial infarction model

In the rat myocardial infarction model, the infarcted myocardium displayed a white hue, accompanied by a disordered myocardial tissue structure and an influx of inflammatory cells (Fig. 1A and B). TUNEL assay depicted the infarcted myocardium with a prominent dark brown hue, suggestive of apoptotic cell presence (Fig. 1C). Elevated levels of myocardial enzyme spectrum indicators, including AST, LDH, CK, CK-MB, and cTnT, were observed in the myocardial cells of infarcted rats (Fig. 1D), confirming the effective establishment of the myocardial infarction model. Concurrently, a diminished expression of miR-182-5p was observed in the infarcted myocardial tissue (Fig. 1E). Post-myocardial infarction, the anti-apoptotic molecule Bcl-2 demonstrated decreased expression, whereas pro-apoptotic molecules, such as Bax, Bnip3, and the apoptosis-executive molecule cleared caspase-3/7, showed enhanced expression. Elevated expression of P53 and the multifunctional apoptosis influencer HIF-1α was also evident (Fig. 1F). Collectively, these data underscore the apoptotic processes instigated by myocardial infarction.

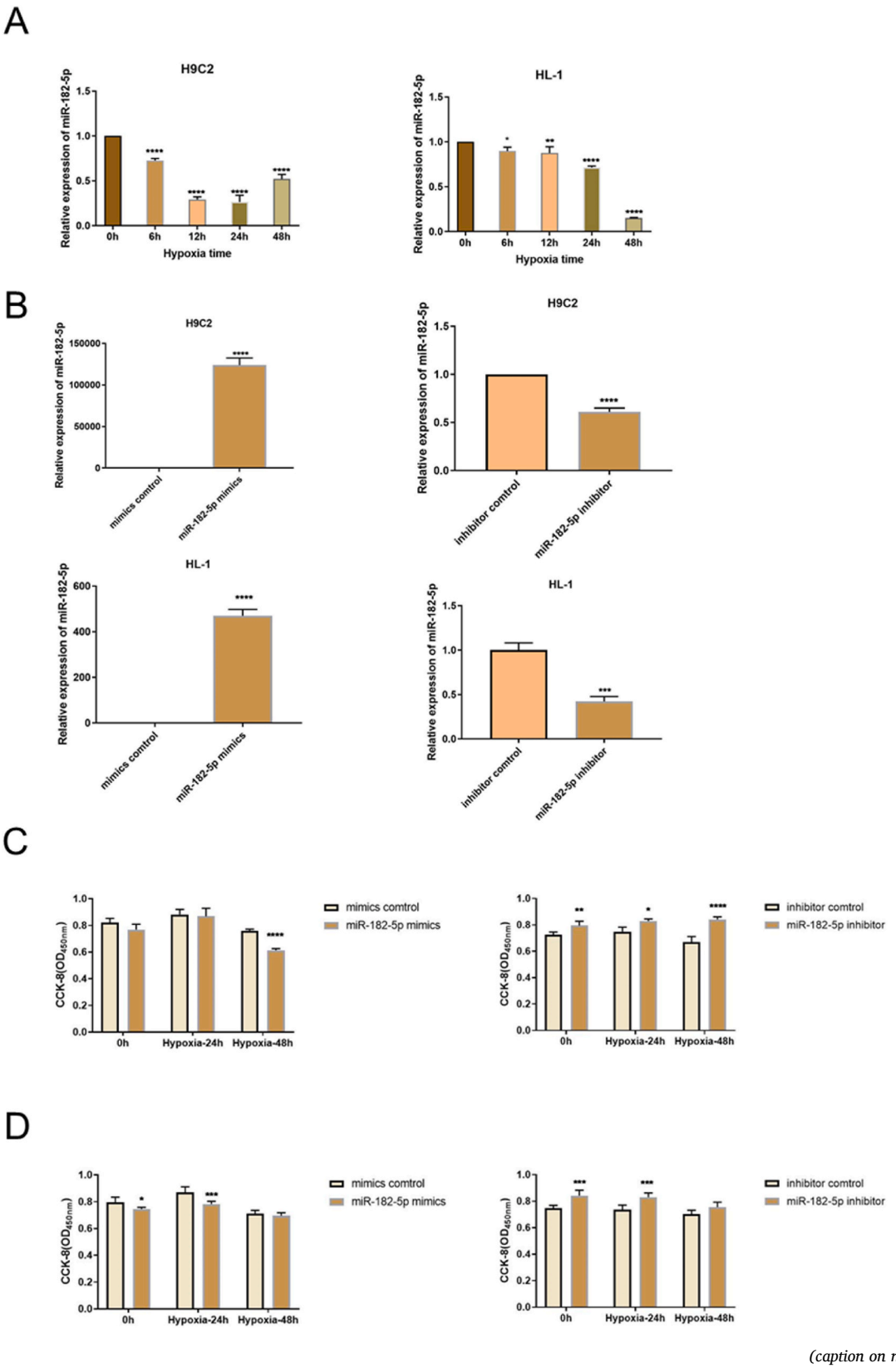

(caption on next page)

Fig. 2. MiR-182-5p's influence on H9C2 and HL-1 cardiomyocyte proliferation under hypoxia. (A) Expression of miR-182-5p in H9C2 and HL-1 cells was detected using qPCR across various hypoxic durations (0, 6, 12, 24, and 48 h). $^{*}P < 0.05$, $^{**}P < 0.01$, $^{****}P < 0.0001$ compared to the 0 h group. (B) Transfection efficiency of miR-182-5p mimics and inhibitor was verified. $^{***}P < 0.001$, $^{****}P < 0.0001$ versus control group. (C, D) MiR-182-5p's effects on H9C2 and HL-1 cell viability were evaluated with the CCK-8 assay. Significant values compared to each bar chart's control group are denoted with "*". $^{*}P < 0.05$, $^{**}P < 0.01$, $^{***}P < 0.0001$, $^{****}P < 0.0001$. Abbreviation: qPCR, quantitative polymerase chain reaction.

3.2. MiR-182-5p effects on the viability of myocardial cells under hypoxia

In the assessment of hypoxic exposure over time, miR-182-5p expression in H9C2 and HL-1 myocardial cells demonstrated a progressive decline, aligning with findings from animal studies (Fig. 2A). Following confirmation of the transfection efficiency of miR-182-5p mimics/inhibitor (Fig. 2B), we analyzed its impacts during various hypoxic intervals (0 h, 24 h, 48 h). The introduction of miR-182-5p mimics markedly suppressed H9C2 cardiomyocyte viability at 48 h of hypoxia, while its inhibition enhanced cell viability at both 24 h and 48 h hypoxic durations (Fig. 2C). In HL-1 myocardial cells, miR-182-5p mimics substantially reduced cell viability under 24 h hypoxia, but its inhibition resulted in augmented cell viability during the same hypoxic period (Fig. 2D). These findings suggest that miR-182-5p exerts a suppressive role in myocardial proliferation.

3.3. MiR-182-5p effects on the apoptosis level of myocardial cells under hypoxia

Overexpression of miR-182-5p in H9C2 cardiomyocytes heightened the caspase-3 activity under hypoxic conditions at both 24 and 48 h intervals. Conversely, inhibiting this miRNA significantly dampened this activity. A parallel trend was confirmed in HL-1 cardiomyocytes (Fig. 3A). In terms of apoptosis-related molecules, overexpressing miR-182-5p notably decreased Bcl-2 expression in myocardial cells under 24 h hypoxia but remained neutral at 48 h. Conversely, inhibition of miR-182-5p upregulated Bcl-2 expression during 24 and 48 h hypoxia.

Upon introducing miR-182-5p mimics, Bax expression increased during 0 and 24 h hypoxia in H9C2 cells and throughout 0, 24, and 48 h in HL-1 cells. Similarly, Bnip3 expression escalated during 0 and 24 h hypoxia for both cell types. In contrast, the miR-182-5p inhibitor downregulated Bax at 48 h in H9C2 and at 0 and 48 h in HL-1 cells. The inhibitor also suppressed Bnip3 expression during 0 and 48 h hypoxia in H9C2 and 0 and 24 h in HL-1 cells.

Furthermore, miR-182-5p modulates multiple apoptotic regulators, with HIF-1α and P53 being particularly influenced. MiR-182-5p mimics bolstered the expression of HIF-1α during 24 h hypoxia in H9C2 and throughout 0, 24, and 48 h in HL-1 cells. The expression of P53 followed a similar pattern. Conversely, the miR-182-5p inhibitor diminished HIF-1α expression at 48 h in H9C2 and 24 h in HL-1, and P53 expression was reduced at 0 and 48 h in H9C2 and 0 and 24 h in HL-1 cells (Fig. 3B and C). In summation, miR-182-5p appears to enhance hypoxic myocardial apoptosis.

3.4. Effects of injection of AAV9-miR-182-5p on the damage from myocardial infarction in mice

The results revealed that following the administration of AAV9-miR-182-5p, the myocardial tissue in mice exhibited vibrant green fluorescence (Fig. 4A). This expression was significantly higher than that observed in the group receiving an empty carrier injection (Fig. B), affirming the successful infection of AAV9-miR-182-5p into mouse myocardial cells. Subsequent to constructing a mouse myocardial infarction model, the injection of AAV9-miR-182-5p notably intensified the extent of myocardial infarction within the myocardial tissue (Fig. 4C).

HE staining results unveiled several distinct characteristics of the infarcted myocardial tissue. These included evident cardiac cavity dilatation, multiple instances of venous congestion and dilatation, the presence of local translucent foreign bodies in the pericardium, and mild connective tissue hyperplasia. Notably, connective tissue hyperplasia was localized in the pericardium, accompanied by slight lymphocyte infiltration. Furthermore, numerous myocardial fibers exhibited necrosis and dissolution, replaced by proliferative connective tissue, and were associated with lymphocyte punctate infiltration. Additionally, localized pericardial edema was observed, characterized by loosely arranged connective tissue and accompanied by limited capillary congestion and dilation (Fig. 4D).

Furthermore, despite the significant increase in myocardial enzymes observed in the infarcted myocardial tissue, the administration of AAV9-miR-182-5p led to a subsequent rise in cTnT, AST, CK, and LDH levels. This suggests that miR-182-5p has the potential to exacerbate myocardial tissue damage during myocardial infarction (Fig. 4E).

The echocardiography results demonstrated that miR-182-5p transfection resulted in a reduction in myocardial ejection fraction, left ventricular short-axis shortening rate (fractional shortening), and an increase in LVPW. These findings indicate that the overexpression of miR-182-5p can, to some extent, augment the abnormalities within myocardial tissue following myocardial infarction (Fig. 4F, Supplementary video).

Finally, we assessed the level of apoptosis in myocardial tissue. The results revealed that AAV9-miR-182-5p significantly reduced the expression of the anti-apoptotic molecule Bcl-2. Concurrently, it elevated the expression levels of pro-apoptotic molecules Binp3, and apoptotic execution molecule caspase-3/7. Interestingly, there was no observable change in the expression of Bax. Notably, we also observed that the overexpression of miR-182-5p led to an increase in the expression of P53 and HIF-1α. These molecules regulate apoptosis pathways through multiple mechanisms (Fig. 5A). Additionally, the results obtained from flow cytometry illustrated a significant increase in the apoptosis rate of myocardial tissue in response to the expression of miR-182-5p (Fig. 5B). Consequently, it is evident that miR-182-5p is a molecule with adverse effects on infarcted myocardium and plays a pivotal role in promoting apoptosis-

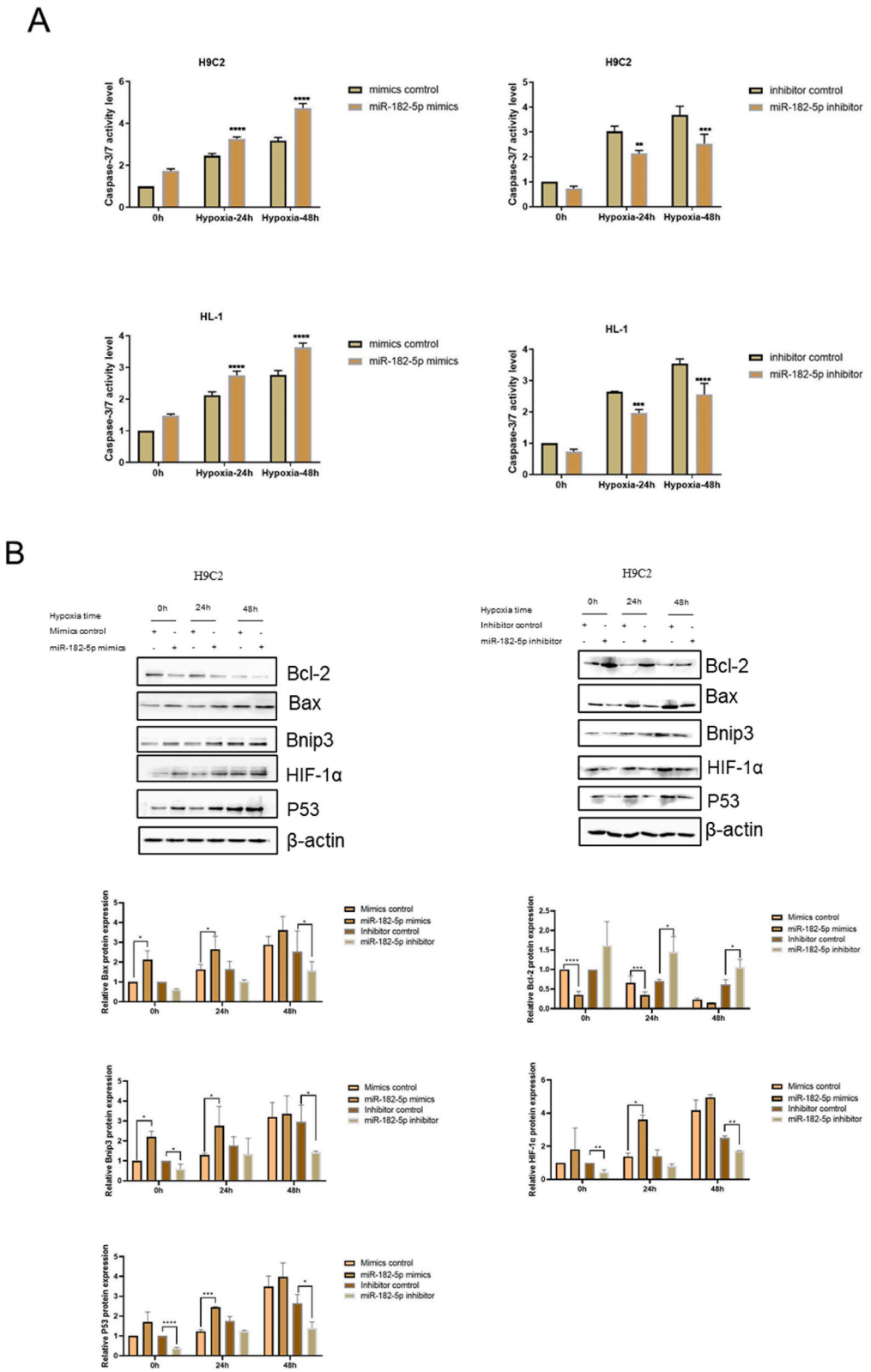

Fig. 3. MiR-182-5p's effect on H9C2 and HL-1 myocardial cell apoptosis under hypoxia. (A) Caspase-3/7 activity in H9C2 and HL-1 cells influenced by miR-182-5p was assessed using the caspase-3/7 activity kit. Significance levels are indicated with "*". $^{**}P < 0.01$, $^{***}P < 0.0001$, $^{****}P <$

0.0001. (B, C) The influence of miR-182-5p on apoptosis-related molecules was evaluated using Western blot analysis. $^{**}P < 0.01$, $^{***}P < 0.001$, $^{****}P < 0.0001$.

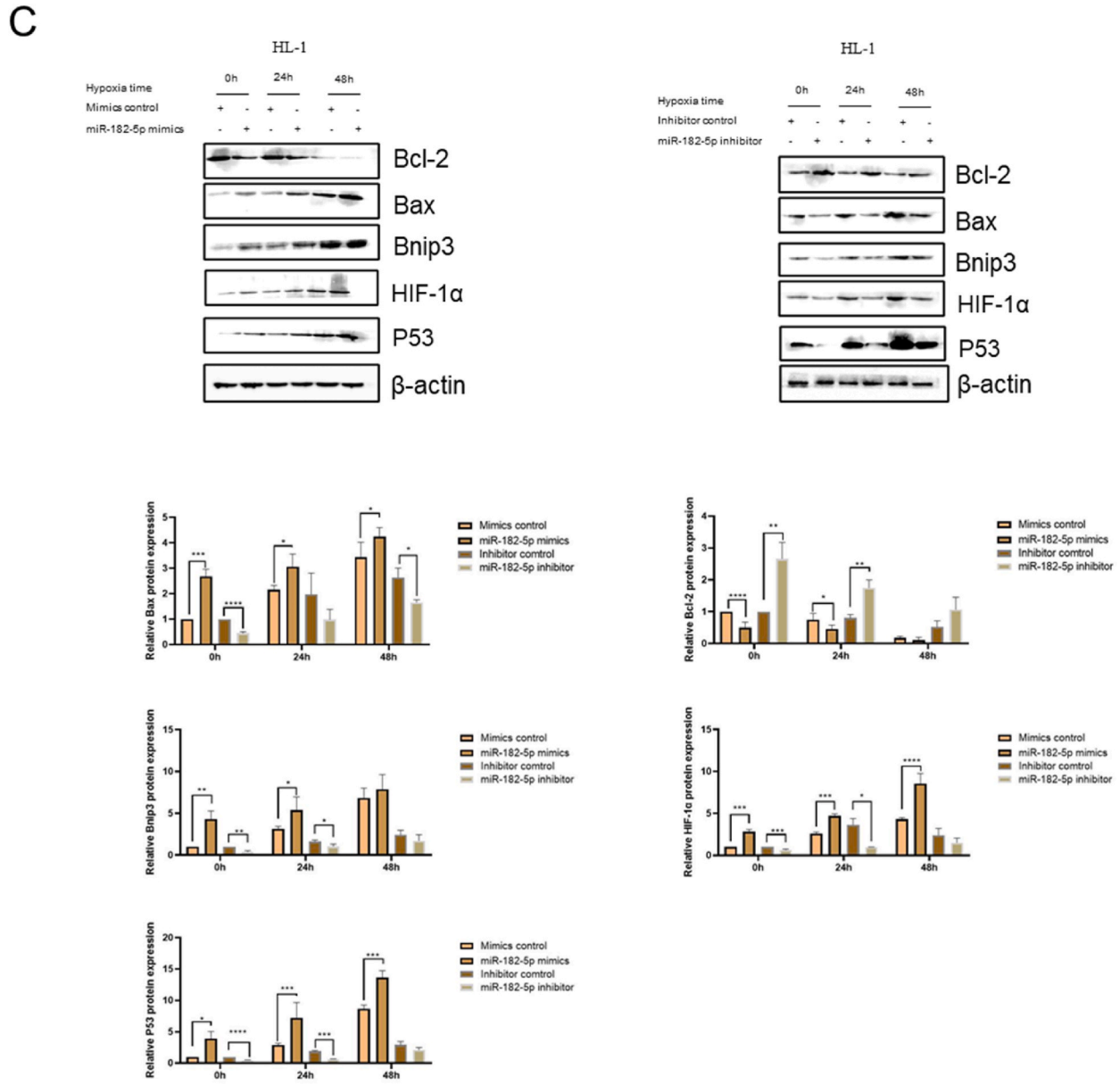

Fig. 3. (*continued*).

related events.

4. Discussion

In our study, we investigated the role of miR-182-5p in myocardial infarction using both in vitro and in vivo models. Contrary to our initial hypothesis of miR-182-5p's protective role, our results demonstrated its exacerbation of myocardial injury and impairment of cardiac function. We posit a 'protectively reduced expression' mechanism, suggesting the body might downregulate miR-182-5p expression to limit myocardial damage. This theory aligns with the understanding that the body often employs protective responses, such as moderating inflammatory reactions, to limit cellular damage during disease. Our findings, consistent across both in vitro and in vivo settings, position miR-182-5p as a significant biomarker for research with potential therapeutic relevance for myocardial infarction management.

MiR-182-5p, consistently expressed in humans and mice, originates from a single primary transcript [13]. It has displayed

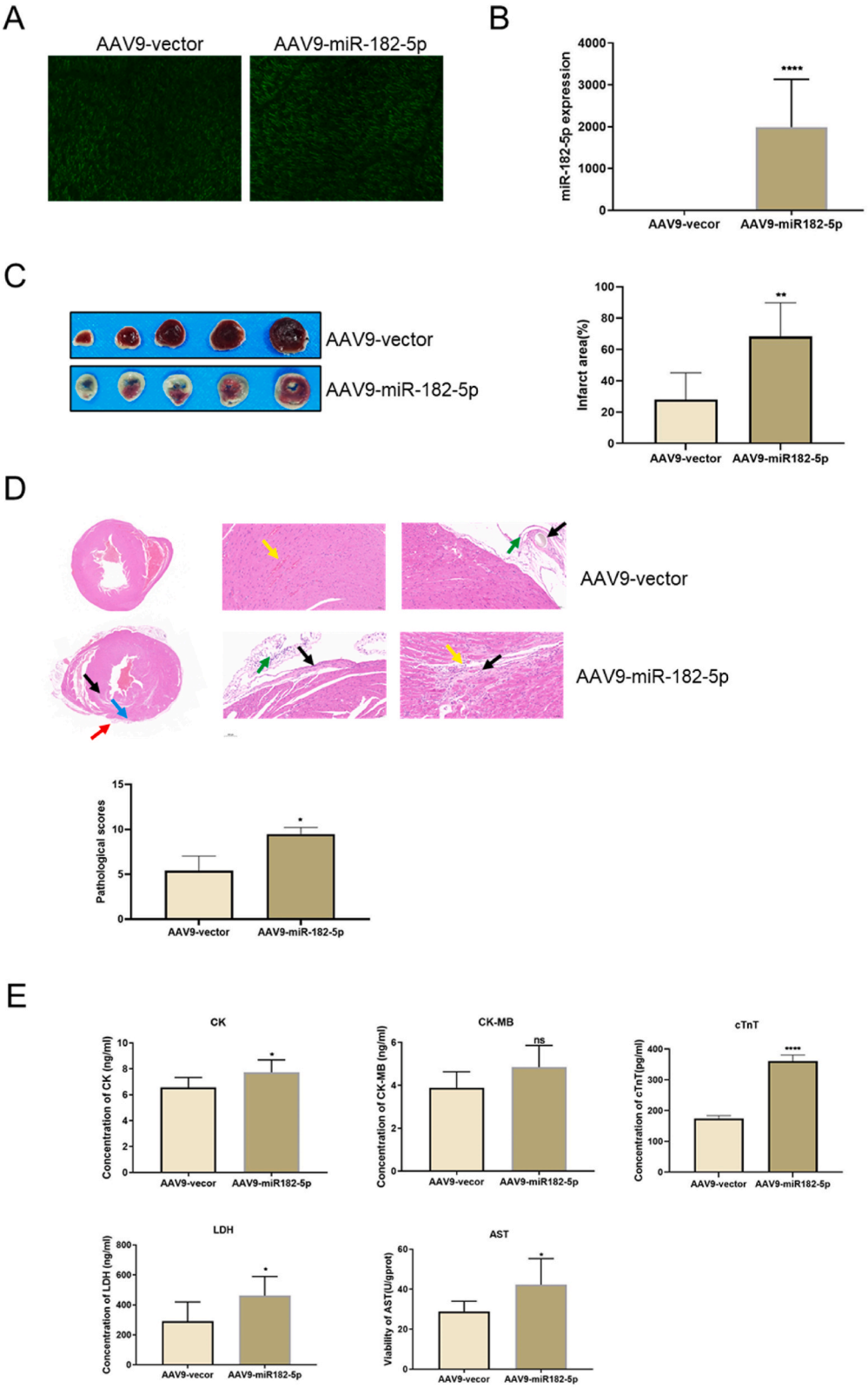

Fig. 4. AAV9-miR-182-5p's role in mouse myocardial infarction injury. (A) Following AAV9 adeno-associated virus injection into the tail vein, myocardial tissue displayed green fluorescence under fluorescence microscopy. (B) MiR-182-5p expression in myocardial tissue was measured using qPCR. (C) TTC method visualized the myocardial infarction area. (D) Myocardial tissue structure was assessed through the HE staining technique,

with 2× and 20× magnifications. Descriptive arrow legends: Black – local translucent foreign bodies and connective tissue alterations; Yellow – mild tissue changes and lymphocyte presence; Red – local pericardial edema and connective tissue characteristics; Blue – capillary features. (E) ELISA quantified myocardial zymogram levels. (F) Echocardiography assessed myocardial function. Results are displayed as mean ± standard deviation (n = 5). Significance markers: $^{*}P < 0.05$, $^{**}P < 0.01$, $^{****}P < 0.0001$ versus the AAV9 vector group. Key abbreviations: ELISA – enzyme-linked immunosorbent assay; HE – hematoxylin eosin; qPCR - quantitative polymerase chain reaction; TTC – 2,3,5-chlorotriphenyltetrazolium. Echocardiographic parameters defined in the legend below: Heart Rate, the number of heartbeats per minute; Diameter_s, ventricular diameter at the end of diastole; Diameter_d, ventricular diameter at the end of systole; Volume_s, ventricular volume at the end of diastole; Volume_d, ventricular volume at the end of systole; Stroke_Volume, the amount of blood pumped out by the left ventricle per heartbeat; Ejection_Fraction, the percentage of ventricular volume pumped out during systole; Fractional_Shortening, the percentage of reduction in ventricular diameter during each heartbeat; Cardiac_Output, the volume of blood pumped out by the left ventricle per minute; LV_Mass, the mass of the left ventricle's myocardium; LV_Mass_Cor, the left ventricle myocardial mass adjusted for body surface area; LVAW_s, Left ventricular anterior wall thickness at diastole; LVAW_d, left ventricular anterior wall thickness at systole; LVPW_s, left ventricular posterior wall thickness at diastole; LVPW_d, left ventricular posterior wall thickness at systole.

differential expression in various cells and conditions, including lymphocytes, sensory organs, and during tumor progression [14–16]. Elevated serum miR-182-5p levels might be a predictive marker for chronic heart failure, offering potential avenues for modulating cardiovascular disease progression [2].

Research on this molecule has encountered challenges due to discrepancies in study findings. For instance, Jia et al. [17] highlighted that suppressing miR-182-5p expression in infarcted myocardium reduces myocardial injury. Yet, other in vitro studies showed that miR-182-5p, when exposed to cobalt chloride, a hypoxia simulant, reduces myocardial apoptosis by targeting Nogo-C. Zhang et al. presented evidence that in in vitro hypoxia experiments, decreasing miR-182-5p expression in H9C2 myocardial cells effectively reduces myocardial injury through CIAPIN1 [7]. Other studies demonstrated varied effects: a decrease in miR-182-5p expression in some cases, while an increase in other scenarios led to cell proliferation and a reduction in apoptosis, as observed with HES1 [18]. Sun et al. introduced a therapeutic approach involving exosomes with miR-182-5p targeting TLR4, a mediator in detrimental inflammatory pathways for infarcted myocardium [9]. These varied findings underline the importance of experimental design and model handling. Notably, while primary myocardial cells offer insights, continuous proliferation in H9C2 and HL-1 myocardial cell lines may affect outcomes.

Extensive experiments using H9C2 and HL-1 cells have focused on hypoxia and related conditions. It's worth noting the differences between these cultured cells and infarcted myocardial tissue. For instance, Kuznetsov et al. found that H9C2 cardiomyocytes more closely resemble primary cardiomyocytes in ATP levels and other parameters than HL-1 cells. Additionally, H9C2 cells are more vulnerable to hypoxia-reoxygenation injury [19], suggesting they might be more apt for in vitro simulations of hypoxia.

However, the transition from in vitro to animal experiments poses challenges, especially considering potential clinical applications on human cells. Our study used both H9C2 and HL-1 myocardial cells to analyze hypoxia gradients. Using AAV9 for viral packaging, we examined the negative effects of miR-182-5p on myocardial function.

Numerous studies connect ischemic cardiomyopathy and specific congenital heart diseases to cell apoptosis [17,20,21]. The consequences of ischemia- and hypoxia-induced myocardial cell apoptosis are severe, leading to adverse cardiac outcomes such as ventricular remodeling [11,22,23]. The exact role of miR-182-5p in these apoptosis pathways remains ambiguous. Bcl-2 proteins play a central role in cell apoptosis regulation [24–26]. While Bcl-2 is known for anti-apoptotic functions, Bax promotes apoptosis through various pathways [27–29]. The balance between these proteins is pivotal in apoptosis inhibition [30,31].

Bnip3, another Bcl-2 protein family member, is predominantly pro-apoptotic. It operates by binding to the mitochondrial outer membrane [32,33]. The relationship between Bnip3 and HIF-1α is especially significant under ischemic and hypoxic conditions, influencing multiple biological processes [34,35].

However, the role of HIF-1α in cardiovascular disease remains a topic of contention [36], While its protective roles in hypoxia are known, prolonged overexpression leads to negative outcomes [37]. This is because HIF-1α influences mitochondrial autophagy [38] and affects the mitochondrial respiratory chain [39], which can eventually cause cell apoptosis [40]. Although direct interactions between miR-182-5p and HIF-1α in cardiovascular contexts are yet to be documented, current research suggests miR-182-5p might influence HIF-1α expression [41].

P53's role in myocardial tissue during ischemia and hypoxia is clear, promoting the expression of pro-apoptotic molecules and impacting the health of infarcted myocardium [20,42,43]. This has led to the development of several P53-targeted inhibitors, showing promise in various applications [20,42,44,45]. Numerous P53-targeted inhibitors have been developed, yet they come with potential cancer risks due to P53's tumor suppressor function. While P53 doesn't directly regulate miR-182-5p [46], our study suggests a potential indirect regulatory mechanism with elevated miR-182-5p levels influencing P53 expression.

This study is not without limitations. We couldn't conduct in vivo evaluations of miR-182-5p expression impacts on rats due to resource constraints. Furthermore, our analysis couldn't pinpoint a miR-182-5p target molecule affecting myocardial apoptosis under hypoxia in all our models. Future research aims to explore miR-182-5p's role during myocardial infarction further.

5. Conclusion

In conclusion, miR-182-5p is not only a significant marker for myocardial apoptosis but also plays a pivotal role in enhancing it. This highlights its potential as a crucial target for both the diagnosis and therapeutic intervention of myocardial infarction. Delving deeper into the exact regulatory mechanism of miR-182-5p on apoptosis-associated molecules will be instrumental for future

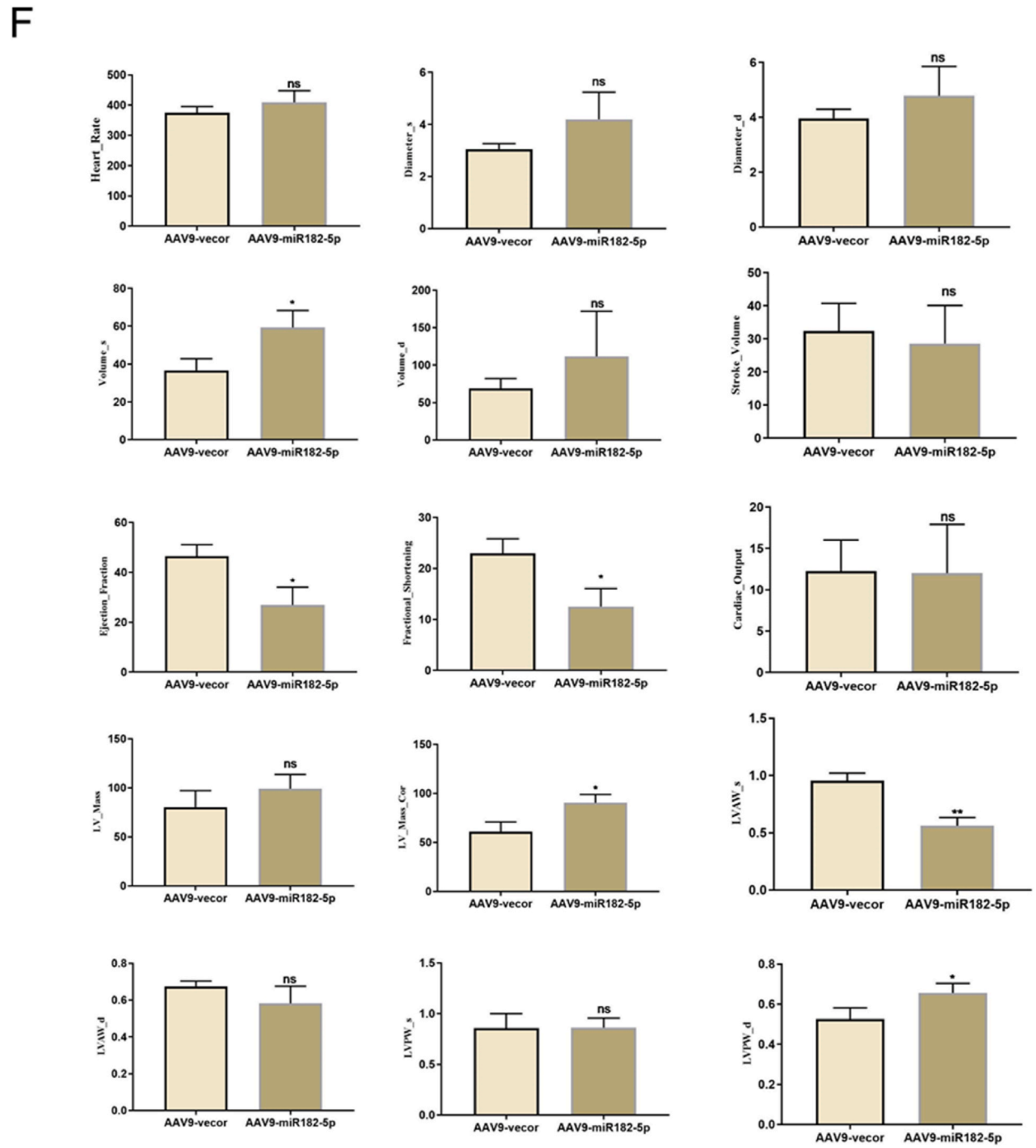

Fig. 4. (*continued*).

myocardial infarction treatments.

Ethical approval

The present study was approved by the Medical Ethics Committee of People's Hospital of Ningxia Hui Autonomous Region (approval no. 2017-016).

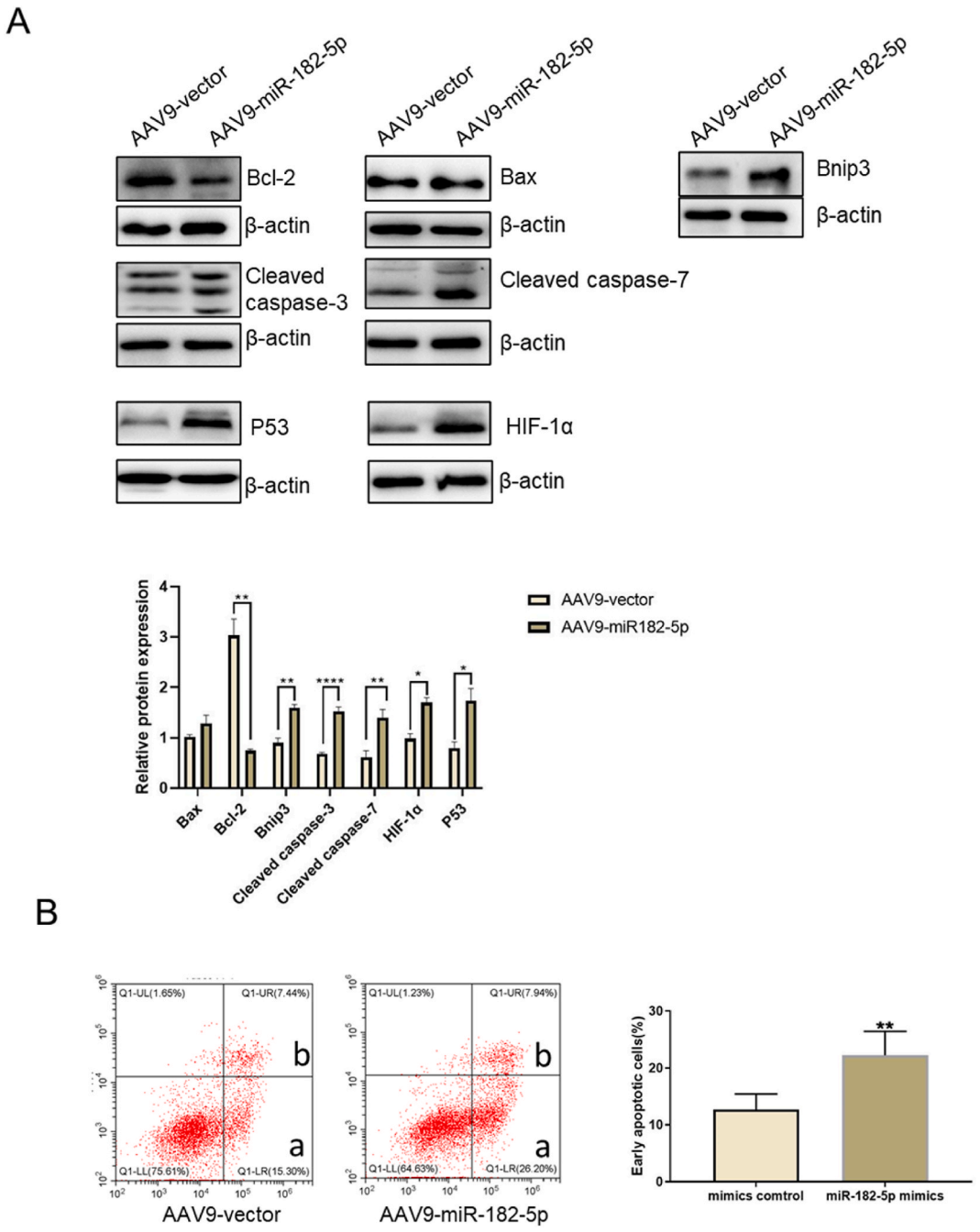

Fig. 5. Impact of AAV9-miR-182-5p on mouse myocardial infarction apoptosis. (A) Expression of several apoptosis-associated proteins in myocardial tissue was determined using Western blot analysis. (B) Flow cytometry evaluated myocardial tissue apoptosis levels, with 'a' indicating early apoptotic cells and 'b' signifying late apoptotic/necrotic cells. The rate of early apoptosis was computed for myocardial tissue apoptosis levels. Data representation: mean ± standard deviation (n = 5), $^{*}P < 0.05$, $^{**}P < 0.01$, $^{****}P < 0.0001$ versus the AAV9 vector group.

Funding

This work was supported by the National Natural Science Foundation [grant number 81760070].

Data availability statement

The data associated with this study has not been deposited in a publicly available repository. The reason for this is the authors do

not have permission to share the data.

Consent for publication

Not applicable.

Availability of supporting data

All data generated or analyzed during this study are included in this published article.

CRediT authorship contribution statement

Nan Niu: Writing – review & editing, Writing – original draft, Software, Methodology, Investigation, Formal analysis, Data curation, Conceptualization. **Huangtai Miao:** Methodology, Investigation, Data curation. **Hongmei Ren:** Project administration, Investigation, Conceptualization.

Declaration of competing interest

The authors declare that they have no known competing financial interests or personal relationships that could have appeared to influence the work reported in this paper.

Acknowledgments

The authors thank the members of the Institute of Medical Sciences of Ningxia Hui Autonomous Region for providing excellent technical assistance. The research was supported by the National Natural Science Foundation of China [Grant Number 81760070]. The authors are grateful for the funding and support received.

Appendix A. Supplementary data

Supplementary data to this article can be found online at https://doi.org/10.1016/j.heliyon.2023.e21524.

References

[1] M. Kayikcioglu, H.S. Ozkan, B. Yagmur, Premature myocardial infarction: a rising threat, Balkan Med. J. 39 (2) (2022) 83–95.
[2] G. Pei, L. Chen, Y. Wang, et al., Role of miR-182 in cardiovascular and cerebrovascular diseases, Front. Cell Dev. Biol. 11 (2023), 1181515.
[3] H.A. Cakmak, E. Coskunpinar, B. Ikitimur, et al., The prognostic value of circulating microRNAs in heart failure: preliminary results from a genome-wide expression study, J. Cardiovasc. Med. 16 (6) (2015) 431–437.
[4] Y. Zhi, C. Xu, D. Sui, et al., Effective delivery of hypertrophic miRNA inhibitor by cholesterol-containing nanocarriers for preventing pressure overload induced cardiac hypertrophy, Adv. Sci. 6 (11) (2019), 1900023.
[5] M.B. Hudson, J.A. Rahnert, B. Zheng, et al., miR-182 attenuates atrophy-related gene expression by targeting FoxO3 in skeletal muscle, Am. J. Physiol. Cell Physiol. 307 (4) (2014) C314–C319.
[6] Y. Liu, J. Dong, B. Ren, MicroRNA-182-5p contributes to the protective effects of thrombospondin 1 against lipotoxicity in INS-1 cells, Exp. Ther. Med. 16 (6) (2018) 5272–5279.
[7] Y. Zhang, J. Fang, H. Ma, Inhibition of miR-182-5p protects cardiomyocytes from hypoxia-induced apoptosis by targeting CIAPIN1, Biochem. Cell. Biol. 96 (5) (2018) 646–654.
[8] X. Li, Y. Jin, Inhibition of miR-182-5p attenuates ROS and protects against myocardial ischemia-reperfusion injury by targeting STK17A, Cell Cycle 21 (15) (2022) 1639–1650.
[9] C. Sun, W. Li, Y. Li, et al., MiR-182-5p mediated by exosomes derived from bone marrow mesenchymal stem cell attenuates inflammatory responses by targeting TLR4 in a mouse model of myocardial infraction, Immune Network 22 (6) (2022) e49.
[10] P. Li, X.-R. Dong, B. Zhang, et al., Molecular mechanism and therapeutic targeting of necrosis, apoptosis, pyroptosis, and autophagy in cardiovascular disease, Chin. Med. J. 134 (22) (2021) 2647–2655.
[11] J. Zhang, X. Zheng, P. Wang, et al., Role of apoptosis repressor with caspase recruitment domain (ARC) in cell death and cardiovascular disease, Apoptosis 26 (1–2) (2021) 24–37.
[12] K.J. Livak, T.D. Schmittgen, Analysis of relative gene expression data using real-time quantitative PCR and the 2(−Delta Delta C(T)) Method, Methods 25 (4) (2001) 402–408.
[13] S. Xu, P.D. Witmer, S. Lumayag, et al., MicroRNA (miRNA) transcriptome of mouse retina and identification of a sensory organ-specific miRNA cluster, J. Biol. Chem. 282 (34) (2007) 25053–25066.
[14] Y. Bai, J. Wang, Y. Chen, et al., The miR-182/Myadm axis regulates hypoxia-induced pulmonary hypertension by balancing the BMP- and TGF-beta-signalling pathways in an SMC/EC-crosstalk-associated manner, Basic Res. Cardiol. 116 (1) (2021) 53.
[15] B. Zhao, M. Luo, A. Wang, et al., MiR-182 antagonist alleviates glucocorticoid-induced secondary bone degeneration and osteoclast differentiation, Cell. Mol. Biol. 67 (5) (2022) 123–130.
[16] Q. Wei, R. Lei, G. Hu, Roles of miR-182 in sensory organ development and cancer, Thorac. Cancer 6 (1) (2015) 2–9.
[17] S. Jia, X. Qiao, J. Ye, et al., Nogo-C regulates cardiomyocyte apoptosis during mouse myocardial infarction, Cell Death Dis. 7 (2016) e2432.
[18] Y. Zhang, B. Peng, Y. Han, MiR-182 alleviates the development of cyanotic congenital heart disease by suppressing HES1, Eur. J. Pharmacol. 836 (2018) 18–24.
[19] A.V. Kuznetsov, S. Javadov, S. Sickinger, et al., H9c2 and HL-1 cells demonstrate distinct features of energy metabolism, mitochondrial function and sensitivity to hypoxia-reoxygenation, Biochim. Biophys. Acta 1853 (2) (2015) 276–284.

[20] Y. Zhang, K. Köhler, J. Xu, et al., Inhibition of p53 after acute myocardial infarction: reduction of apoptosis is counteracted by disturbed scar formation and cardiac rupture, J. Mol. Cell. Cardiol. 50 (3) (2011) 471–478.
[21] N. Liu, Y. Zhu, W. Song, et al., Cardioprotection attributed to aerobic exercise-mediated inhibition of ALCAT1 and oxidative stress-induced apoptosis in MI rats, Biomedicines 10 (9) (2022) 2250.
[22] X. Chang, R. Liu, R. Li, et al., Molecular mechanisms of mitochondrial quality control in ischemic cardiomyopathy, Int. J. Biol. Sci. 19 (2) (2023) 426–448.
[23] X. Lu, B. Yang, R. Qi, et al., Targeting WWP1 ameliorates cardiac ischemic injury by suppressing KLF15-ubiquitination mediated myocardial inflammation, Theranostics 13 (1) (2023) 417–437.
[24] F. Edlich, BCL-2 proteins and apoptosis: recent insights and unknowns, Biochem. Biophys. Res. Commun. 500 (1) (2018) 26–34.
[25] D.R. Green, The mitochondrial pathway of apoptosis Part II: the BCL-2 protein family, Cold Spring Harbor Perspect. Biol. 14 (6) (2022), a041046.
[26] L. Lu, J. Dong, L. Wang, et al., Activation of STAT3 and Bcl-2 and reduction of reactive oxygen species (ROS) promote radioresistance in breast cancer and overcome of radioresistance with niclosamide, Oncogene 37 (39) (2018) 5292–5304.
[27] Y. Zhang, X. Yang, X. Ge, et al., Puerarin attenuates neurological deficits via Bcl-2/Bax/cleaved caspase-3 and Sirt3/SOD2 apoptotic pathways in subarachnoid hemorrhage mice, Biomed. Pharmacother. 109 (2019) 726–733.
[28] T. Moldoveanu, P.E. Czabotar, A coming of age for the BCL-2 family effector proteins, BAX, BAK, and BOK, Cold Spring Harbor Perspect. Biol. 12 (4) (2020) a036319.
[29] P. Wolf, A. Schoeniger, F. Edlich, Pro-apoptotic complexes of BAX and BAK on the outer mitochondrial membrane, Biochim. Biophys. Acta Mol. Cell Res. 1869 (10) (2022), 119317.
[30] H. Azimian, M. Dayyani, M.T.B. Toossi, et al., Bax/Bcl-2 expression ratio in prediction of response to breast cancer radiotherapy, Iran. J. Basic Med. Sci. 21 (3) (2018) 325–332.
[31] N.A. Helaly, N.E. Esheba, D.E.A. Ammo, et al., High Bax/Bcl-2 ratio is associated with good prognosis and better survival in patients with B cell chronic lymphocytic leukemia, Leuk. Res. 107 (2021), 106604.
[32] J. Zhang, P.A. Ney, Role of BNIP3 and NIX in cell death, autophagy, and mitophagy, Cell Death Differ. 16 (7) (2009) 939–946.
[33] X. Zheng, T. Zhong, Y. Ma, et al., Bnip3 mediates doxorubicin-induced cardiomyocyte pyroptosis via caspase-3/GSDME, Life Sci. 242 (2020), 117186.
[34] Z.-J. Fu, Z.-Y. Wang, L. Xu, et al., HIF-1alpha-BNIP3-mediated mitophagy in tubular cells protects against renal ischemia/reperfusion injury, Redox Biol. 36 (2020), 101671.
[35] Y. Zhang, D. Liu, H. Hu, et al., HIF-1alpha/BNIP3 signaling pathway-induced-autophagy plays protective role during myocardial ischemia-reperfusion injury, Biomed. Pharmacother. 120 (2019), 109464.
[36] C.R. Datta, A. Banik, B. Mandal, et al., Cardiac-specific overexpression of HIF-1alpha during acute myocardial infarction ameliorates cardiomyocyte apoptosis via differential regulation of hypoxia-inducible pro-apoptotic and anti-oxidative genes, Biochem. Biophys. Res. Commun. 537 (2021) 100–108.
[37] M. Hölscher, K. Schäfer, S. Krull, et al., Unfavourable consequences of chronic cardiac HIF-1alpha stabilization, Cardiovasc. Res. 94 (1) (2012) 77–86.
[38] X. Yue, P. Zhao, K. Wu, et al., GRIM-19 inhibition induced autophagy through activation of ERK and HIF-1alpha not STAT3 in Hela cells, Tumour Biol. 37 (7) (2016) 9789–9796.
[39] X.-L. Zhao, C.-Z. Yu, Vosaroxin induces mitochondrial dysfunction and apoptosis in cervical cancer HeLa cells: involvement of AMPK/Sirt3/HIF-1 pathway, Chem. Biol. Interact. 290 (2018) 57–63.
[40] X. Zhao, L. Liu, R. Li, et al., Hypoxia-Inducible factor 1-alpha (HIF-1alpha) induces apoptosis of human uterosacral ligament fibroblasts through the death receptor and mitochondrial pathways, Med. Sci. Monit. 24 (2018) 8722–8733.
[41] Y. Li, D. Zhang, X. Wang, et al., Hypoxia-inducible miR-182 enhances HIF1alpha signaling via targeting PHD2 and FIH1 in prostate cancer, Sci. Rep. 5 (2015), 12495.
[42] T. Yano, K. Abe, M. Tanno, et al., Does p53 inhibition suppress myocardial ischemia-reperfusion injury? J. Cardiovasc. Pharmacol. Therapeut. 23 (4) (2018) 350–357.
[43] K.-M. Liu, H.-H. Zhang, Y.-N. Wang, et al., Wild-type p53-induced phosphatase 1 deficiency exacerbates myocardial infarction-induced ischemic injury, Chin. Med. J. 130 (11) (2017) 1333–1341.
[44] Z. Xu, D. Lu, J. Yuan, et al., Storax attenuates cardiac fibrosis following acute myocardial infarction in rats via suppression of AT1R-ankrd1-P53 signaling pathway, Int. J. Mol. Sci. 23 (21) (2022), 13161.
[45] A.T. Naito, S. Okada, T. Minamino, et al., Promotion of CHIP-mediated p53 degradation protects the heart from ischemic injury, Circ. Res. 106 (11) (2010) 1692–1702.
[46] Y. Liu, W. Qiang, X. Xu, et al., Role of miR-182 in response to oxidative stress in the cell fate of human fallopian tube epithelial cells, Oncotarget 6 (36) (2015) 38983–38998.